ELSEVIER

Journal of Nuclear Materials 318 (2003) 157–166

journal of nuclear materials

www.elsevier.com/locate/jnucmat

Effects of mercury on fatigue behavior of Type 316 LN stainless steel: application in the spallation neutron source

H. Tian [a,*], P.K. Liaw [a], J.P. Strizak [b], L.K. Mansur [b]

[a] *Department of Materials Science and Engineering, The University of Tennessee, Knoxville, TN 37996-2200, USA*
[b] *Metals and Ceramics Division, Oak Ridge National Laboratory, P.O. Box 2008, Oak Ridge, TN 37831-6151, USA*

Abstract

The high-cycle fatigue behavior of Type 316 stainless steel (SS), the prime candidate target-container material for the spallation neutron source (SNS), was investigated in air and mercury at frequencies of 0.2 and 10 Hz with a R ratio of -1, and at 10 and 700 Hz with a R ratio of 0.1. Here R equals the ratio of the applied minimum to maximum loads during fatigue experiments. A decrease in the fatigue life in mercury was observed, relative to that in air, at 0.2 Hz. Correspondingly, intergranular fracture was found on the fracture surfaces of specimens tested in mercury at 0.2 Hz, which is a typical fracture mode caused by liquid metal embrittlement (LME). Heating by mechanical working was observed during fatigue tests at 10 Hz and a R of -1, and at 700 Hz and a R of 0.1, which resulted in great increases in specimen temperatures and shorter fatigue lives for large stress amplitudes ($\geqslant 210$ MPa), relative to those in mercury. However, in the fatigue tests at 10 and 700 Hz, the fatigue lives in air with cooling and those in mercury seemed to be comparable, indicating little influence of the mercury. Thus, both specimen self-heating and LME need to be considered in understanding fatigue behavior of Type 316 SS in air and mercury.

1. Introduction

The candidate target container material of the spallation neutron source (SNS) is Type 316 low-carbon, nitrogen-added (LN) stainless steel (SS). The research and development program for the target, with emphases on the materials aspects, is described in Ref. [1]. The main damage mechanisms on the container are radiation effects and pressure waves caused by the pulsed proton beam (~0.7 μs pulse length, 60 Hz). However, most mechanical test data on 316 LN SS have been accumulated in monotonic loading conditions, and relatively less information for fatigue loading conditions is available [2–7]. Furthermore, there is little information on fatigue behavior of structural material, including 316 LN SS, in mercury environments [4–12].

In this investigation, a series of load-controlled fatigue tests were performed in air and mercury using a state-of-the-art high-frequency electrohydraulic machine operated at 700 Hz and a second machine operated at lower frequencies [4–7]. The prime goal of the present work is to determine whether liquid metal embrittlement (LME) can occur and affect mechanical behavior of the alloy in contact with mercury.

2. Experimental procedure

Type 316 LN SS is an austenitic stainless steel with the chemical composition shown in Table 1 [13]. The material was melted in an electric-furnace, subjected to an argon-oxygen decarburization process (EF/AOD) and met the American Society of Mechanical Engineers (ASME) NCA3800 QSC-245 specification [13]. The material was annealed at 1038 °C for 1 h.

Round-bar specimens were used for fatigue tests with R ratios of -1 and 0.1, where $R = \sigma_{min}/\sigma_{max}$, σ_{min} and σ_{max} are the applied minimum and maximum stresses, respectively. The geometries of the round-bar

* Corresponding author.
E-mail address: htian@utk.edu (H. Tian).

0022-3115/03/$ - see front matter
doi:10.1016/S0022-3115(03)00116-8

Table 1
Chemical composition of Type 316 low-carbon, nitrogen-added (LN) stainless steel (SS) (wt%, weight percent)

Element	C	Mn	P	S	Si	Ni	Cr	Mo	Co	Cu	N	Fe
wt%	0.009	1.75	0.029	0.002	0.39	10.2	16.31	2.07	0.16	0.23	0.11	Bal.

specimens used are illustrated in Figs. 1 and 2. The specimens for fatigue tests with a R ratio of −1 had a total length of 228.60 mm, a gage length of 20.32 mm, and a diameter of 7.62 mm. The specimens for fatigue tests with a R ratio of 0.1 had a total length of 118.8 mm, a gage length of 19.0 mm, and a diameter of 5.1 mm. In order to conduct fatigue tests in a mercury environment, a container of 304 SS was attached to

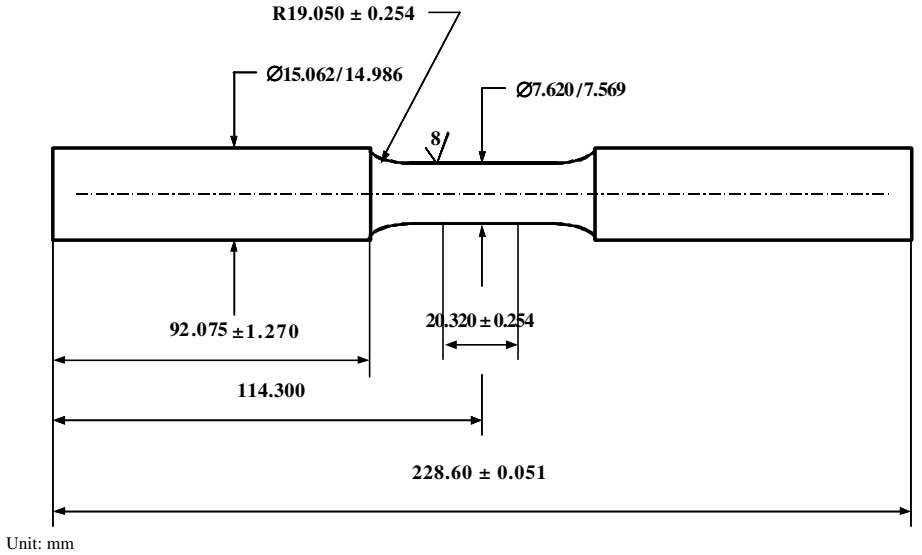

Fig. 1. Cylindrical specimen used for HCF tests at a R ratio of −1.

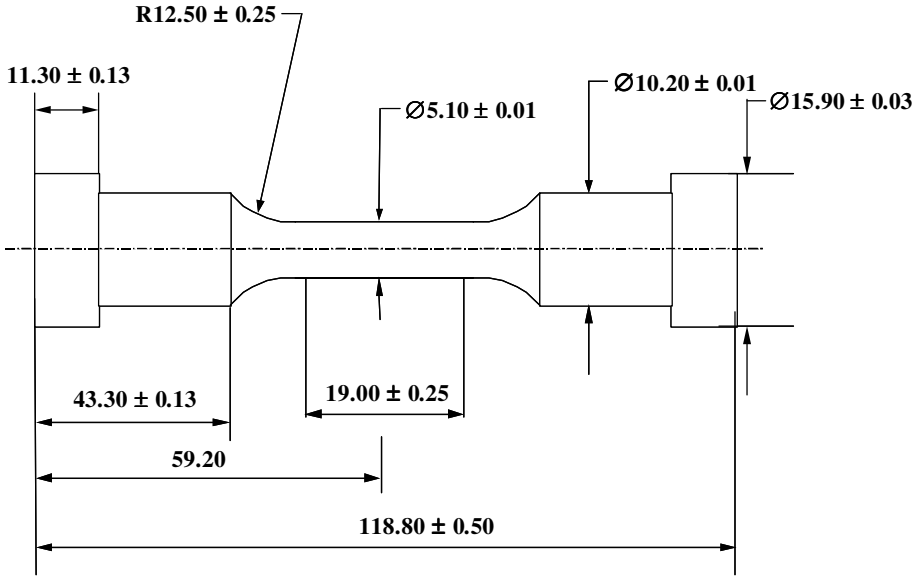

Fig. 2. Cylindrical specimen used for HCF tests at a R ratio of 0.1.

each specimen. The gage section of the specimen was immersed in mercury enclosed in the container. The container had a height of 48 mm and an inner diameter of 17 mm. The container was attached to the specimen with a silicone-rubber adhesive sealant, which allowed the container to be removed from the specimen after the test, and reused.

Two state-of-the-art electrohydraulic material test systems (MTS) were used in the present study. One has a frequency range from 0.001 to 60 Hz. It was used to run tests at 0.2 and 10 Hz. The second machine is an advanced, high-frequency, electrohydraulic MTS machine with a frequency range from 20 to 1000 Hz and a loading capacity of ±25 KN. Servovalves are activated by voice coils to achieve frequencies up to 1000 Hz. To avoid testing noise at 1000 Hz, the machine is situated in a well-designed, soundproof room equipped with a heat pump, which has the cooling capability to prevent overheating of the servovalves. Several fatigue tests were conducted to approximately 10^9 cycles at 700 Hz. A sinusoidal wave was employed during fatigue tests, which has a strain rate roughly estimated to be in the range of 0.03 and 3.89 s^{-}. The pressure wave loads of SNS in operation are expected to be lower than 150 MPa at 60 Hz, which has a strain rate of about 0.1 s^{-}.

In the mercury-environment fatigue tests, an airflow system (Model MINI-PAC) was used to absorb the mercury vapor, and clean the air near the specimen to eliminate the possibility of mercury entering the room. Following the fatigue tests in mercury, the specimens were cleaned in acetone with an ultrasonic cleaning machine (Model FS20) for 1 h.

For some fatigue tests that need to cool down the specimens because of heat generation during cyclic loading, a cooling apparatus that used low-temperature nitrogen gas was designed. The low-temperature gas was obtained by passing nitrogen gas through a dewar containing liquid nitrogen. Fig. 3 illustrates the fatigue testing equipment with the specimen-cooling apparatus made up of a dewar, a conducting tube, and a cooling ring. The cooling ring has an inner diameter of 15.7 mm and a height of 41.4 mm. Two thermocouples were used to monitor the temperature of the test sample. One was mounted on the surface of the specimen, and the other was fixed near the specimen to monitor the temperature of the outlet liquid-nitrogen gas around the specimen.

A water-cooling line was used to provide active cooling for fatigue tests in mercury. A copper coil was wound around the mercury container, and water circulation was used to remove heat from the container during fatigue tests, which reduced the specimen temperature.

A high-speed and high-sensitivity, thermography-infrared detection method was also employed to observe changes in the specimen temperature during fatigue [14–19]. This technique uses infrared radiation emitted from the surface of a material to determine its temperature. The equipment employed in the experiment is a state-of-the-art, high-resolution, Raytheon-Radiance-HS infrared (IR) imaging system – an IR camera, which has a temperature resolution up to 10^{-2} °C and a spatial resolution of 5.4 μm. Under the snapshot mode, the IR camera has a tunable data-acquisition speed up to 6100 Hz, and was used to measure the specimen temperature during fatigue

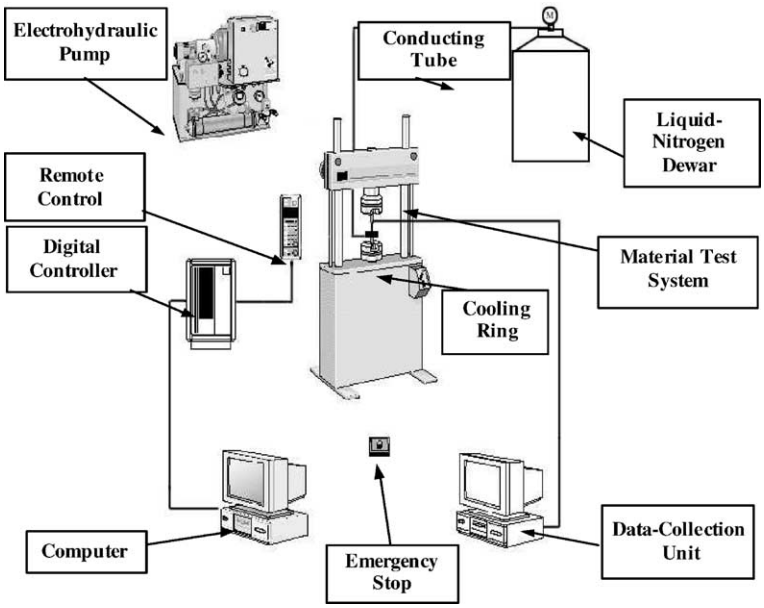

Fig. 3. MTS with nitrogen cooling.

testing. A thin sub-micron graphite coating was applied on the specimen gage-length section of the as-machined sample in order to reduce IR reflections and increase the thermal emissivity of the specimen surface. The coating was applied on the surface of the container when the specimen was surrounded by the container, and the temperature of the container was measured.

The cooling apparatus was started before the beginning of the fatigue tests. The nitrogen gas continuously flowed over the surface of the specimen. The nitrogen pressure was manually controlled. High-cycle fatigue (HCF) tests were conducted under load control in air and mercury with the stress amplitude (σ_a) ranging from approximately 125 to 250 MPa at a R ratio of 0.1, and from 190 to 290 MPa at a R ratio of -1. Note that $\sigma_a = (\sigma_{max} - \sigma_{min})/2$. The test procedure was in accordance with the American Society for Testing and Materials (ASTM) E466 on 'Conducting Constant Amplitude Axial Fatigue Tests of Metallic Materials' [20].

The curves of stress amplitudes (σ_a) versus number of cycles to failure (N_f) [i.e., S–N curves] were developed in air and mercury. Following fatigue tests, a scanning-electron microscope (SEM), Model Cambridge S-360, was employed to observe the fracture surfaces and study fracture mechanisms.

3. Results

3.1. $R = -1$

3.1.1. At 0.2 Hz

The test results are shown in Fig. 4. Considering the fact that fatigue data have large scatter, the fatigue lives at 0.2 Hz in mercury are comparable with those in air. However, at stress amplitudes above 230 MPa, fatigue tests at 0.2 Hz in mercury generally exhibited shorter lives to a certain extent, as compared with those in air, with the exception of stress levels of 236 and 263 MPa, where some fatigue tests in air and mercury showed comparable cycles to failure. Similar fatigue endurance limits at stress amplitudes of about 210 and 220 MPa were observed for tests in air and mercury.

The fatigue test data were fitted statistically according to the ASTM E739 for 'Standard Practice for Statistical Analysis of Linear or Linearized Stress-Life (S–N) and Strain-Life (ε–N) Fatigue Data'. Assuming a linear S–N relationship exists [21],

$$S = A \log N_f + B, \quad (1)$$

in which S and N_f refer to the amplitude of the cyclic stress and the number of cycles to failure, respectively, and A and B are fitting constants. The fits are shown by lines on the figures, such as Fig. 4. The run-out data represents specimens that did not fail and were suspended after a certain number of cycles. The fits do not involve the run-out data. Horizontal lines were drawn out according to the run-out data, indicating the fatigue endurance limits.

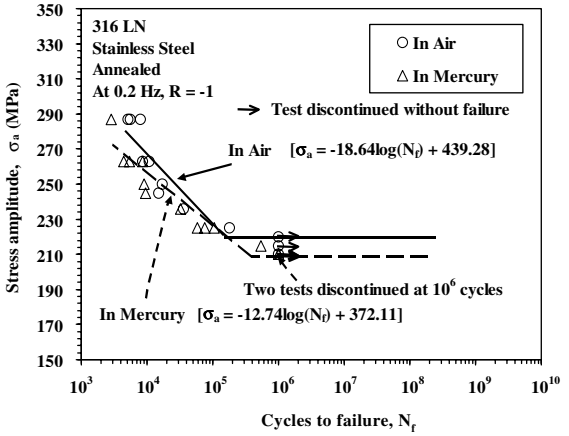

Fig. 4. Environmental effect on the fatigue life of 316 LN SS at 0.2 Hz and a R ratio of -1.

3.1.2. At 10 Hz

Fig. 5 presents the fatigue lives in air and mercury at 10 Hz. Shorter fatigue lives as well as a lower fatigue endurance limit were measured in air than in mercury at 10 Hz. For the fatigue test at 10 Hz and $\sigma_a = 263$ MPa, the specimen temperature in air was much greater than that in mercury, approximately 334 versus 130 °C, which decreased yield strength, and thus, the fatigue life in air (Table 2). Note that increasing temperature decreases yield strength in Table 2. By decreasing the specimen temperature to a range of 20–60 °C with nitrogen cooling, longer fatigue lives were observed in air than in mercury (Fig. 5), which was caused by a relative higher

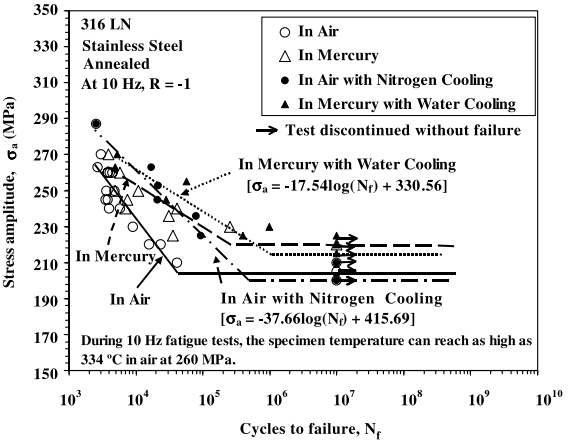

Fig. 5. Environmental effect on the fatigue life of 316 LN SS at 10 Hz and a R ratio of -1 with nitrogen and water cooling.

Table 2
Tensile properties of 316 LN SS at a strain rate of 0.001 s^{-}

Specimen condition	Test temperature (°C)	$\sigma_{0.2}$ (MPa)	σ_{uts} (MPa)
Annealed	24	289	600
	300	173	460
	500[a]	133	350

$\sigma_{0.2}$ = 0.2% offset yield strength.
σ_{uts} = ultimate tensile strength.
[a] From Ref. [13].

temperature in mercury, approximately 130 °C in mercury versus 20–60 °C in air. Moreover, the fatigue lives in air with nitrogen cooling were longer than those in air without nitrogen cooling. By controlling the specimen temperature in air with nitrogen cooling and in mercury with water cooling, comparable fatigue lives were measured at 10 Hz (Fig. 5) with similar specimen temperatures in air and mercury in the range of 20–60 °C, although somewhat shorter fatigue lives were observed in mercury at higher stress (⩾ 260 MPa).

3.2. $R = 0.1$

3.2.1. At 10 Hz

Fig. 6 shows the effect of test environment on fatigue life at 10 Hz. There was no specimen self-heating effect at 10 Hz in air with a R ratio of 0.1. The specimen temperature remained at room temperature throughout the test at all the stress levels. Fatigue tests at the stress amplitude greater than 210 MPa in mercury at 10 Hz have shorter lives as compared with those in air (Fig. 6). However, for tests at lower stress levels (<210 MPa), the material has comparable fatigue lives in mercury and air.

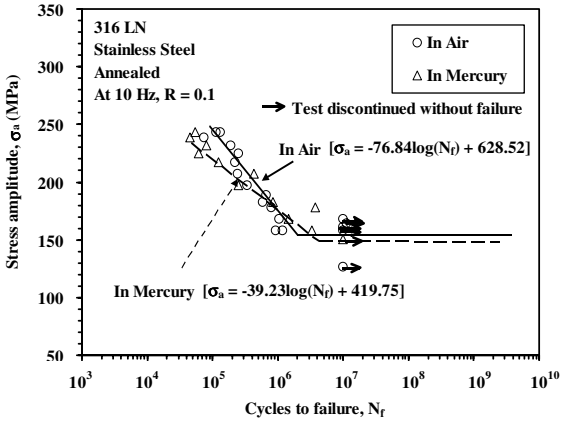

Fig. 6. Environmental effect on the fatigue life of 316 LN SS at 10 Hz and a R ratio of 0.1.

3.2.2. At 700 Hz

Fig. 7 presents the S–N curves at 700 Hz in air and mercury. Longer fatigue lives in mercury than in air were observed. This trend was caused by the specimen self-heating at 700 Hz, which produced a much higher specimen temperature in air than in mercury. As shown in Fig. 8, the specimen temperature in air seemed to increase linearly with increasing test frequency. A similar phenomenon was observed for fatigue tests in mercury. However, mercury around the specimen served as a cooling medium. As a result, the specimen temperature only rose to 78 °C in mercury (Fig. 8). At higher temperatures, the yield strength of 316 LN SS decreases (Table 2), which results in lower fatigue resistance.

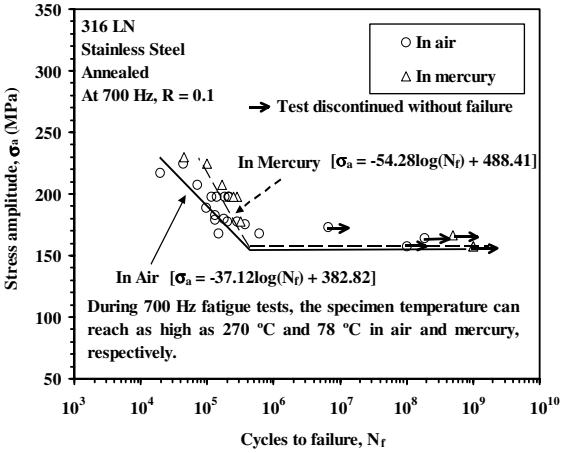

Fig. 7. Environmental effect on the fatigue life of 316 LN SS at 700 Hz and a R ratio of 0.1.

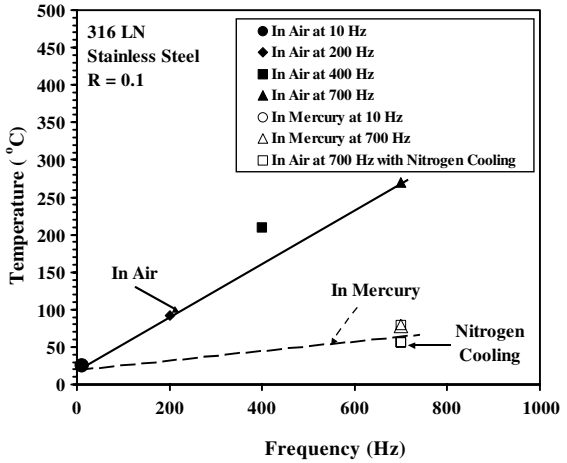

Fig. 8. Variation of the specimen temperature with the test frequency during fatigue experiments of 316 LN SS in air and mercury at a stress amplitude of 198 MPa and a R ratio of 0.1.

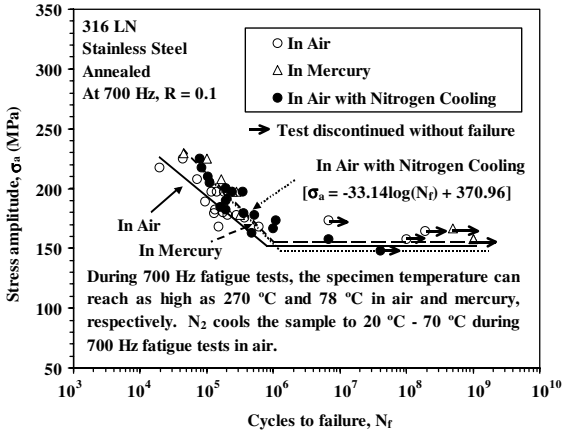

Fig. 9. Environmental effect on the fatigue life of 316 LN SS at 700 Hz and a R ratio of 0.1.

Comparable fatigue lives in air and mercury were measured after cooling the specimen in air using nitrogen gas, as shown in Fig. 9, because of the comparable specimen temperatures in cool nitrogen gas and mercury (Fig. 8).

3.3. Fractography

3.3.1. $R = -1$

The fracture surface of specimens tested in air and mercury showed a significant difference in fracture modes, especially in the crack-propagation region. Specimens tested in air exhibited typical transgranular (TG) cracking in the crack-propagation region at 0.2 and 10 Hz (Figs. 10 and 11), while those in mercury showed some intergranular (IG) cracking at high stress levels ($\geqslant$ 230 MPa) (Figs. 12 and 13). At lower stress levels (<230 MPa) in mercury, IG cracking can also be seen on the fracture surfaces, but the amount of IG sites is much less than that at high stress levels.

3.3.2. $R = 0.1$

The SEM micrographs of the fracture surfaces of the fatigue specimens tested in air and mercury at a R ratio of 0.1 showed different fracture mechanisms, especially in the crack-growth region of the fatigue fracture surface. Figs. 14 and 15 are micrographs of the typical crack-propagation region of 316 LN SS tested in air and mercury at 10 Hz, respectively. The specimen tested in air showed typical TG cracking throughout most of the fracture surface (Fig. 14). In contrast, the specimen

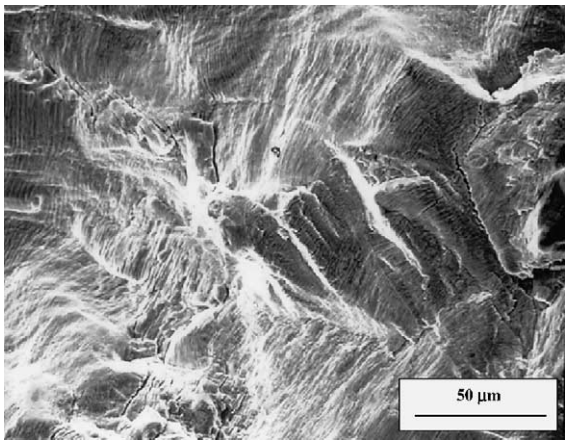

Fig. 11. Fracture surface showing the TG fracture in the crack-propagation area. The specimen was a 316 LN SS tested in air at 10 Hz with a stress amplitude of 260 MPa and a R ratio of −1.

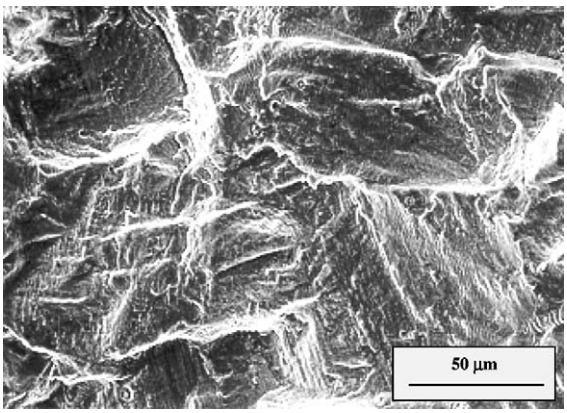

Fig. 10. Fracture surface showing the TG fracture in the crack-propagation area. The specimen was a 316 LN SS tested in air at 0.2 Hz with a stress amplitude of 260 MPa and a R ratio of −1.

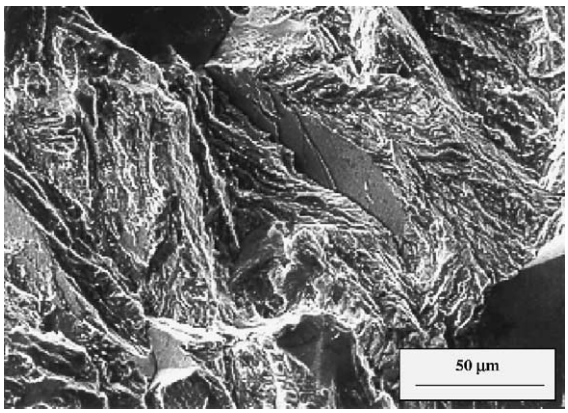

Fig. 12. Fracture surface showing the IG fracture in the crack-propagation area. The specimen was a 316 LN SS tested in mercury at 0.2 Hz with a stress amplitude of 260 MPa and a R ratio of −1.

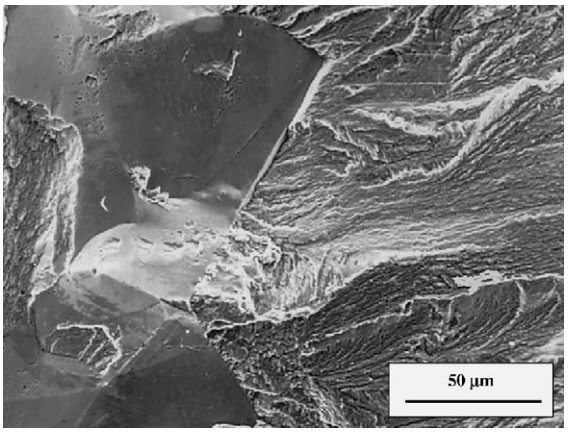

Fig. 13. Fracture surface showing the IG fracture in the crack-propagation area. The specimen was a 316 LN SS tested in mercury at 10 Hz with a stress amplitude of 260 MPa and a R ratio of −1.

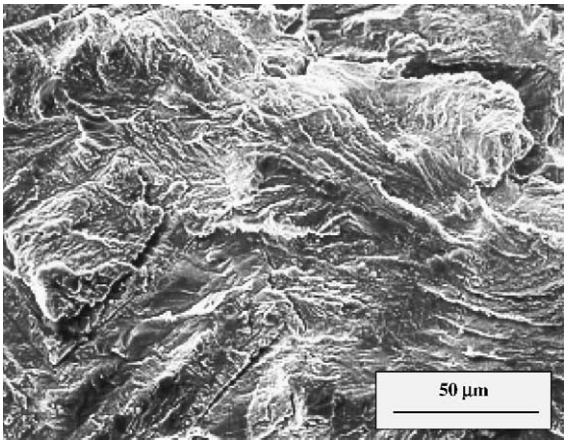

Fig. 14. Fracture surface showing the typical fracture mode in the crack-propagation area. The specimen was a 316 LN SS tested in air at 10 Hz with a stress amplitude of 232 MPa and a R ratio of 0.1.

tested in mercury exhibited IG cracking at high stress levels ($\geqslant$ 210 MPa), as presented in Fig. 15. At lower stress levels (<210 MPa) in mercury, IG cracking can rarely be seen on the fracture surfaces. The IG cracking region is believed to be a direct result of LME. TG fracture was the typical mode observed in air and mercury at 700 Hz.

4. Discussion

In the past, LME was studied mainly using uniaxial tension tests or slow-strain-rate tension tests, rather than by cyclic loading tests [8–11]. Several materials tested in

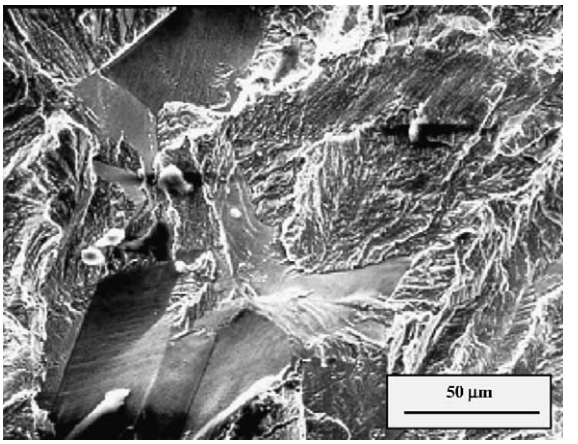

Fig. 15. Fracture surface showing the IG fracture in the crack-propagation area. The specimen was a 316 LN SS tested in mercury at 10 Hz with a stress amplitude of 232 MPa and a R ratio of 0.1.

mercury were found to exhibit more brittle fracture characteristics than in air [9–11]. Some research results exhibited similar fracture modes of nickel-based alloys in gaseous hydrogen and liquid mercury, while other results reported that the fracture features were distinguishable in these two conditions, with more IG cracking in mercury than hydrogen [9–11]. LME was found to be more severe in nickel and copper alloys than in steels because of the limitation of wetting between the mercury and steel [11].

Interestingly, although many papers reported significant LME effects on other alloys, little research indicated obvious LME effects on stainless steels. LME effects are widely observed in copper, aluminum alloys, and nickel alloys, when they are subjected to the corrosion effect of the mercury environment for a long time of service. Related LME phenomena are documented in several papers [8–12]. This process of LME produces a drastic reduction in the fracture resistance of the solid, but has no apparent changes in its yield or flow behavior. Nevertheless, this effect has not been widely observed in steels.

Pawel et al. investigated the corrosion behavior of 316 LN SS in a mercury thermal convection loop [22]. Two thermal convection loops fabricated from 316 LN SS, containing mercury (Hg) and Hg with 1000 wppm gallium (Ga), respectively, were operated continuously for about 5000 h [22]. In each case, the maximum loop temperature was constant at about 305 °C, and the minimum temperature was maintained at approximately 242 °C. Coupons in the hot leg of the Hg-loop developed a porous surface layer substantially depleted of nickel and chromium, which resulted in a transformation to ferrite [22]. Analysis of the corrosion-rate data as a function of temperature in the Hg-loop suggests that

wetting by mercury occurred only above about 255 °C, and that the rate-limiting step in the corrosion process above 255 °C is solute diffusion through the saturated mercury boundary layer adjacent to the corroding surface. Experimental results suggest no obvious LME effect in the Hg-loop that contributes to the degradation of coupons. The main mechanism that induced the depletion of elements is diffusion.

Classical LME processes are generally found to occur without the notable penetration of the embrittling species into the solid or the dissolution of the solid metal into the embrittling liquid. Various other liquid metal degradation phenomena were reviewed elsewhere, such as grain-boundary penetration, selective attack of solid phases, or reactions between the solid and liquid [10].

During fatigue tests in the mercury environment, the specimens are subjected to cyclic loading, and there also exists the processes of crack initiation and propagation. Therefore, the loading condition would become another important factor besides the temperature effect mentioned above. With the occurrence of crack initiation and propagation, the interaction between the mercury penetrating into the crack tip and the plastic zone area of the crack tip becomes more obvious. Under different loading conditions, the depths of penetration of mercury into the crack are different due to various levels of openings of a crack.

4.1. $R = -1$

4.1.1. At 0.2 Hz

For fatigue tests at stress levels above 230 MPa, although the fatigue lives in air and mercury are overall comparable, but there are still differences in fatigue lives in air and mercury at almost all the stress levels tested (Fig. 4). Fatigue lives in mercury are relatively shorter than in air except at two stress levels, as discussed previously. Thus, LME is suggested to be the main factor that contributes to the somehow shorter fatigue life of 316 LN SS (Fig. 4) in mercury, relative to that in air. At higher stress levels, mercury has more chance to interact directly with the fresh surface in the crack-tip area due to the larger plastic deformation, which exhibited the characteristic IG fracture in Fig. 12.

4.1.2. At 10 Hz

With comparable specimen temperatures in air and mercury after cooling, comparable fatigue lives were found in air and mercury (Fig. 5), although somewhat shorter fatigue lives in air at stress levels below 260 MPa were observed. The small difference in the fatigue lives is most likely caused by the insufficient cooling using nitrogen gas at 10 Hz, compared to the cooling by water for fatigue tests in mercury. As discussed above, even though the specimen was cooled using nitrogen gas, the specimen temperature in air after cooling is still higher than room temperature, which could have caused a bit shorter lives in air. The shorter lives in mercury with water cooling than in air with nitrogen-gas cooling at stress levels above 260 MPa was due to the environmental effect, as evidenced by the presence of the IG fracture in mercury (Fig. 13).

4.2. $R = 0.1$

4.2.1. At 10 Hz

For fatigue tests at higher stress levels (e.g., $\geqslant 210$ MPa), LME is supposed to be the main factor that decreases the fatigue life of 316 LN SS (Fig. 6). The environmental effect is more significant at higher stress levels, which can be explained with regard to the greater plastic deformation. The maximum stress level (σ_{max}) at a R ratio of 0.1 is 540 MPa, which is well above the yield strength of the material (289 MPa). This means during the first half-cycle, the extensive plastic deformation damages the chromium oxide scale on the specimen and exposes the fresh metal surface to the mercury, which facilitates the LME process. At higher stress levels, mercury may have more chance to interact directly with the fresh surface in the crack-tip area. Thus, there is a greater possibility of better contact of the mercury with the fresh metal surface at higher stresses. Moreover, at higher stress levels, the fatigue life is generally determined by the crack-propagation process. During the crack-growth period at higher stress levels, the crack-opening displacement (COD) is relatively large, which facilitates the penetration of mercury into the crack tip and the contact with the fresh crack surface. Correspondingly, the penetration depth of the mercury may be increased during a higher stress fatigue test, and wetting of the freshly cracked surface by mercury may be enhanced. These trends result in the LME effects of mercury at higher stress levels, characteristic of the presence of the IG fracture (Fig. 15).

At low stress levels (<210 MPa), the fatigue lives in mercury are comparable to those in air as presented in Fig. 6. This trend is a combination of the result of the lack of the penetration and wetting of mercury at low stresses, which decreased LME.

4.2.2. At 700 Hz

Thermography results showed that temperature might be the dominant factor that contributed to the difference in the fatigue life at 700 Hz in air and mercury (Fig. 7). For the fatigue test at 700 Hz and $\sigma_a = 198$ MPa with a R ratio of 0.1, the specimen temperature in air was much greater than that in mercury, approximately 270 versus 78 °C (Fig. 8). Mercury serves as a heat sink and effectively lowers the specimen temperature at 700 Hz, which results in longer fatigue lives in mercury than air. In Fig. 9, similar fatigue lives were measured in air and mercury at 700 Hz by controlling

Table 3
Environmental effects on the fatigue behavior of 316 LN SS

Effects	Condition	Phenomenon	Mechanism
$R = -1$	0.2 Hz	Shorter fatigue lives in mercury than in air	LME effect
	10 Hz	Significant shorter fatigue lives in air than in mercury	Greater specimen temperature in air than in mercury; mercury acting as a coolant, reducing the specimen temperature
$R = 0.1$	10 Hz	Shorter fatigue lives in mercury than in air	LME effect; better wetting between the mercury and steel
	700 Hz	Longer fatigue lives in mercury than in air	Insignificant LME effect; greater specimen temperature in air than in mercury

the specimen temperature to a range of 58–78 °C using the cool nitrogen gas in air.

In Fig. 7, decreasing the stress level decreases the difference in the fatigue lives in air and mercury. This trend can be expected to result from the fact that decreasing the stress reduces the specimen temperature in air [14–19], which yields a reduced difference in the fatigue lives in air and mercury.

5. Conclusions

(1) For tests at 0.2 Hz with a R ratio of -1 in mercury at stress amplitudes above 230 MPa, the fatigue life was shorter than in air. Below 230 MPa, fatigue lives in air and mercury were comparable. The effect at high stresses is attributed to LME (Table 3).

(2) Without water cooling, fatigue tests at 10 Hz with a R ratio of -1 had shorter lives in air than in mercury due to the temperature effect. With cooling, fatigue tests at 10 Hz in mercury at stress amplitudes above 260 MPa showed shorter lives than in air. Below 260 MPa, fatigue lives in air and mercury were comparable.

(3) For tests at 10 Hz with a R ratio of 0.1 and stress amplitudes above 210 MPa, the fatigue lives are shorter in mercury than in air. For lower stress amplitudes, the results were comparable. The effect at higher stress levels is attributed to LME.

(4) For tests at 700 Hz with a R ratio of 0.1, the fatigue lives in air with nitrogen cooling are comparable with those in mercury. LME is minimal at 700 Hz.

(5) IG fracture was the typical cracking mode in mercury at 0.2 and 10 Hz with a R ratio of -1 at stress amplitudes above 230 MPa. Below 230 MPa in mercury, IG cracking can also be seen on the fracture surfaces, but the amount of IG sites was much less than that at higher stress levels. TG fracture was observed in air at 0.2 and 10 Hz.

(6) For fatigue tests at a R ratio of 0.1, IG fracture was the typical cracking mode in mercury at 10 Hz with stress amplitudes above 210 MPa. Below 210 MPa in mercury, TG fracture was the typical cracking mode. TG fracture was observed in air at 10 Hz, as well as in air and mercury at 700 Hz.

(7) Above all, the present study indicated that the presence of mercury did not generally decrease the endurance limit of Type 316 LN stainless steel in the test conditions investigated.

Acknowledgements

This research was sponsored by the Division of Materials Sciences and Engineering, Office of Basic Energy Science, US Department of Energy under contract DE-AC05-00OR22725 with the UT-Battelle, LLC.

References

[1] L.K. Mansur, T.A. Gabriel, J.R. Haines, D.C. Lousteau, J. Nucl. Mater. 296 (2001) 1.
[2] M. Botshekan, S. Degallaix, Y. Desplanques, Mater. Sci. Eng. A 234–236 (1997) 463.
[3] J.B. Vogt, J. Foct, C. Regnard, G. Robert, J. Dhers, Metall. Trans. A 22A (1991) 2385.
[4] H. Tian, P.K. Liaw, H. Wang, D. Fielden, J.P. Strizak, L.K. Mansur, J.R. DiStefano, Mater. Sci. Eng. A 314 (1–2) (2001) 140.
[5] H. Tian, P.K. Liaw, D. Fielden, L. Jiang, B. Yang, C.R. Brooks, D.D. Bruns, M.D. Brotherton, H. Wang, J.P. Strizak, L.K. Mansur, J.R. DiStefano, K. Farrell, D.C. Lousteau, S.J. Pawel, G.T. Yahr, in: P.K. Liaw (Ed.), Proceedings of Symposium on Fatigue and Fracture Behavior of High Temperature Materials, The TMS/ASM Fall Meeting, St. Louis, Missouri, 8–12 October 2000, The Minerals, Metals, and Materials Society, 2000, p. 37.
[6] J.P. Strizak, J.R. DiStefano, P.K. Liaw, H. Tian, J. Nucl. Mater. 296 (2001) 225.
[7] H. Tian, P.K. Liaw, D. Fielden, C.R. Brooks, M.D. Brotherton, J.P. Strizak, L.K. Mansur, J.R. DiStefano Jr., K. Farrell, Asdfs sd fksdjfk, in: D.R. Lesuer, T.S. Srivatsan (Eds.), Proceedings of Symposium on Modeling the Performance of Engineering Structural Materials, The TMS/ASM Fall Meeting, Indianapolis, Indiana, 4–8 November

2001, The Minerals, Metals, and Materials Society, 2001, p. 161.
[8] C.E. Price, J.K. Good, Trans. of the Amer. Soci. of Mech. Eng. (ASME) 106 (1984) 178.
[9] J.J. Krupowicz, J. Eng. Mater. Tech. 111 (1989) 229.
[10] C.E. Price, L.B. Traylor, Natl. Assoc. Corr. Eng. 43 (1987) 1639.
[11] D.A. Wheeler, R.G. Hoagland, J.P. Hirth, Corrosion 45 (1989) 207.
[12] J.A. Kapp, D. Duquette, M.H. Kamdar, J. Eng. Mater. Tech. 108 (1986) 37.
[13] R.W. Swindeman, ORNL/NPR-92/24, June 1993.
[14] H. Wang, L. Jiang, P.K. Liaw, D.L. Klarstrom, Metall. Mater. Trans. A 31 (2000) 1307.
[15] L. Jiang, H. Wang, P.K. Liaw, C.R. Brooks, D.L. Klarstrom, Metall. Mater. Trans. A 32 (9) (2001) 2279.
[16] B. Yang, P.K. Liaw, H. Wang, L. Liang, J.Y. Huang, R.C. Kuo, J.G. Huang, Mater. Sci. Eng. 314 (1–2) (2001) 131.
[17] P.K. Liaw, H. Wang, L. Jiang, B. Yang, J.Y. Huang, R.C. Kuo, J.G. Huang, Scr. Mater. 42 (2000) 389.
[18] H. Wang, L. Jiang, Y.H. He, L.J. Chen, P.K. Liaw, R.R. Seeley, D.L. Klarstrom, Metall. Mater. Trans. A 33 (4) (2002) 1287.
[19] L. Jiang, H. Wang, P.K. Liaw, C.R. Brooks, D.L. Klarstrom, Trans. Nonferrous Metals Soc. China 12 (4) (2002) 734.
[20] Annual Book of ASTM Standards, vol. 03.01, 2000, p. E466-91.
[21] Annual Book of ASTM Standards, vol. 03.01, 2000, p. E739-91.
[22] S.J. Pawel, J.R. DiStefano, E.T. Manneschmidt, ORNL/TM-13754, 1999.